Coupled Systems Mechanics, *Vol. 13, No. 3 (2024) 187-200*
https://doi.org/10.12989/csm.2024.13.3.187

Buckling analysis of piles in weak single-layered soil with consideration of geometric nonlinearities

Emina Hajdo[1a], Emina Hadzalic[*1] and Adnan Ibrahimbegovic[2b]

[1]*Faculty of Civil Engineering, University of Sarajevo, 71000 Sarajevo, Bosnia and Herzegovina*
[2]*Université de Technologie de Compiègne-Alliance Sorbonne Université, Centre de Recherche, 60200 Compiègne, France*

(Received January 22, 2024, Revised February 26, 2024, Accepted February 27, 2024)

Abstract. This paper presents a numerical model for buckling analysis of slender piles, such as micropiles. The model incorporates geometric nonlinearities to provide enhanced accuracy and a more comprehensive representation of pile buckling behavior. Specifically, the pile is represented using geometrically nonlinear beams with the von Karman deformation measure. The lateral support provided by the surrounding soil is modeled using the spring approach, with the spring stiffness determined according to the undrained shear strength of the soil. The numerical model is tested across a wide range of pile slenderness ratios and undrained shear strengths of the surrounding soil. The numerical results are validated against analytical solutions. Furthermore, the influence of various pile bottom end boundary conditions on the critical buckling force is investigated. The implications of the obtained results are thoroughly discussed.

Keywords: buckling; geometric nonlinearities; micropile; pile; spring; stiffness; undrained shear strength; von Karman; weak soil

1. Introduction

The consideration of buckling instability in pile design is often deemed unnecessary, particularly for piles fully embedded in soil, due to the perceived low risk of its occurrence. The prevailing belief is that even weak soil provides adequate lateral support, thereby eliminating the possibility of pile buckling. This assumption, however, may not universally hold true, as factors such as soil type, pile slenderness, and applied loads can influence the potential for buckling (Bergfelt 1957, Gabr *et al.* 1994, Sabatini *et al.* 2005).

Pile buckling in weak soils, such as soft clays, refers to the potential instability and lateral deflection of a pile under axial loads in soil conditions where the lateral support provided by the surrounding soil is insufficient to prevent buckling. Design code EN 1997-1 mandates a buckling assessment for soils with an undrained shear strength (c_u) below 10 kPa, while DIN 1054 requires

*Corresponding author, Assistant Professor, E-mail: emina.hadzalic@gf.unsa.ba
[a]Assistant Professor, E-mail: emina.hajdo@gf.unsa.ba
[b]Professor, E-mail: adnan.ibrahimbegovic@utc.fr

Copyright © 2024 Techno-Press, Ltd.
http://www.techno-press.org/?journal=csm&subpage=8 ISSN: 2234-2184 (Print), 2234-2192 (Online)

such an assessment for undrained shear strength values below 15 kPa. According to these design codes, the occurrence of buckling failure is considered unlikely for higher values of undrained shear strength. However, this assertion does not apply to slender piles, such as micropiles (Bruce *et al.* 2005, Vogt *et al.* 2009). The use of micropiles is becoming more and more widespread due to their suitability for projects located in areas with restricted access, such as urban environments or sites with limited equipment maneuverability. However, owing to their relatively small diameter (d), typically less than 300 mm, and lengths (L) of up to 20-30 m, micropiles may be susceptible to buckling due to their high slenderness ratio (L/d), ranging up to 300 (Gato and Montrasio 2021).

The buckling of piles can be classified into two groups (Bhattacharya *et al.* 2005). The first group involves local buckling, where the deformation primarily occurs within the cross-section of the pile, leading to localized damage. The second group deals with global buckling, where a significant portion or the entire length of the pile undergoes longitudinal deformation, resulting in lateral instability reminiscent of Euler buckling observed in unsupported struts. Global buckling becomes a significant concern in long and slender piles in weak soils, particularly when subjected to significant axial loads.

The critical force at which the pile under axial compression becomes unstable and buckle is greater than the theoretical Euler critical force for an unsupported strut due to the lateral support provided by the surrounding soil. Therefore, when assessing the critical force for buckling failure of piles, this lateral support, which helps to stabilize the pile against buckling by providing resistance to lateral movement, has to be considered.

The critical buckling force assessment for piles has previously been carried out by employing both analytical and numerical methods. Analytically, piles are often treated as beams on elastic foundations (Engesser 1889, Timoshenko and Gere 1961), with lateral support from surrounding soil modeled using discrete linear elastic springs. The springs may have constant stiffness or stiffness that linearly increases with depth (Davisson 1963, Prakash 1987). Several studies determined spring stiffness by correlating it with the undrained shear strength of the surrounding soil (Poulos and Davis 1980, Reese *et al.* 2000). Furthermore, an analytical method accommodating arbitrary end conditions and realistic variations in both soil stiffness and shaft friction is introduced (Heelis *et al.* 2004). To enhance these analytical models, a mathematical approach that accounts for soil nonlinearity and second-order effects has been proposed (Vogt *et al.* 2009). Further exploration into the buckling load and post-buckling behavior of piles is investigated using a nonlinear large deflection differential equation (Zhao *et al.* 2010). A noteworthy contribution to the field has been made by analysing the influence of active and passive earth pressures on the critical buckling load (Chen *et al.* 2013). In addition, a variational approach utilizing the Rayleigh-Ritz direct method and Fourier development of soil stiffness along the pile for buckling analysis is suggested (Fenu *et al.* 2021).

Apart from analytical approaches, numerous studies commonly employ numerical methods to analyse pile buckling. For instance, the critical buckling force has been computed using the small bending theory and the finite-difference method (Hegazy 2014). Furthermore, numerical models employing the finite element method with either a spring or continuum approach to model single-layered or multi-layered soil, have been widely utilized (Ofner and Wimmer 2007, Shatri *et al.* 2014, Nadeem *et al.* 2015, Salama and Basha 2019, Gatto and Montrasio 2021). Several works have specifically focused on the buckling analysis of piles in soil prone to liquefaction, such as (Knappett and Madabhushi 2009, Zhang *et al.* 2020, Tang *et al.* 2021). It is noteworthy that certain numerical studies mentioned earlier incorporate the consideration of geometric nonlinearities in their analyses, such as (Nadeem *et al.* 2015, Zhang *et al.* 2020, Tang *et al.* 2021).

To conduct a more comprehensive pile buckling analysis, it is imperative to consider geometric nonlinearities. By incorporating these nonlinearities into the analysis, the model becomes more adept at capturing the intricate interactions between the pile and the surrounding soil, leading to a more enhanced understanding of the buckling phenomenon.

Various beam finite elements have been developed and tested to ensure their effectiveness in representing geometrically nonlinear behavior, such as (Ibrahimbegovic and Frey 1993, Jelenić and Crisfield 1999, Meier *et al.* 2019, Masjedi *et. al* 2019, Imamovic *et al.* 2019, Mejia-Nava *et al.* 2022, Tojaga *et al.* 2023), among others. These elements offer a versatile and comprehensive approach to accurately model and analyse a wide range of structural responses.

Piles play a crucial role in supporting various structures, emphasizing the need for a comprehensive understanding of their buckling behavior. This paper presents a refined numerical model designed to evaluate the critical buckling force of the pile. A key aspect of the proposed model lies in the representation of the pile using beam elements, offering the capability to account for geometrically nonlinear behavior. Specifically, the von Karman deformation measure is incorporated with an aim to accurately capture the complexities arising from geometric nonlinearities (Ibrahimbegovic *et al.* 2013, Hajdo *et al.* 2022). The numerical representation of the surrounding soil involves utilizing a spring model, in which the soil is represented as a series of linear elastic springs. The stiffness of each spring in the model is determined based on correlations with the undrained shear strength of the soil.

The outline of the paper is as follows: Section 2 provides a short overview of the analytical solution for the pile critical buckling force. In Section 3, the theoretical formulation of the geometrically nonlinear beam finite element, which allows for a more realistic and efficient modeling of pile buckling behavior, is explained in more detail. In Section 4, the results of several numerical simulations are presented and compared with analytical solutions for different pile slenderness ratios and different values of undrained shear strength of surrounding soil. The influence of pile bottom end boundary conditions on the critical buckling force is also investigated. Concluding remarks are given in Section 5.

2. Analytical solution through analogy with a beam on an elastic foundation

The classical approach to obtain critical buckling force for a pile is closely related to the problem of a beam on an elastic foundation, specifically a Winkler foundation (Fig. 1).

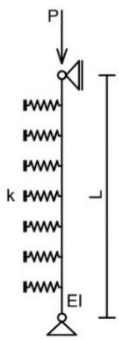

Fig. 1 Pile supported by springs representing stiffness of the surrounding soil

In this context, the surrounding soil is modeled as discrete, linear elastic springs, accounting for the soil stiffness and its influence on the buckling behavior of the pile. The differential equation governing the problem is given as

$$EI\frac{d^4u_y}{dx^4} + P\frac{d^2u_y}{dx^2} + ku_y = 0 \tag{1}$$

where E is Young's modulus of elasticity of the pile, I is the second moment of inertia of the pile, u_y is the lateral displacement of the pile, P is the axial force on the pile, and k is the soil stiffness.

The analytical solution for the critical buckling force of a pile is equal to (Engesser 1889)

$$P_{cr,i} = n^2\left(\frac{\pi}{L}\right)^2 EI + \frac{1}{n^2}\left(\frac{L}{\pi}\right)^2 k \tag{2}$$

where L is the length of the pile, and n is the integer number representing the buckling mode, i.e., the number of sinusoidal semi-waves in a buckled form of the pile.

The critical buckling force of a pile consists of two parts. The first part pertains to the Euler critical force at which buckling of unsupported pile occurs. The second part accounts for the increase in the critical buckling force of a pile due to the lateral support provided by the surrounding soil. The critical buckling force of a pile P_{cr} is determined as the minimum value obtained from Eq. (2).

For higher values of pile length, the critical buckling force can be evaluated using the following expression (Engesser 1889)

$$P_{cr} = 2\sqrt{EIk} \tag{3}$$

3. Finite element formulation

When addressing issues related to geometric instability, numerous structural analyses predominantly concentrate on buckling, which considers small deformations before reaching a critical equilibrium state. In such scenarios, it becomes feasible to maintain linear kinematics and only introduce nonlinear equilibrium equations (Ibrahimbegovic 2009). In this context, we present a finite element formulation for a two-dimensional Euler-Bernoulli beam element, incorporating the von Karman deformation measure (Hajdo *et al.* 2020, Hajdo *et al.* 2021).

The von Karman deformation measure for an Euler-Bernoulli beam is defined as

$$\varepsilon^{vk} = \frac{du_x}{dx} + \frac{1}{2}\left(\frac{du_y}{dx}\right)^2 - y\frac{d^2u_y}{dx^2} \tag{4}$$

where u_x is axial displacement, and u_y is the transverse displacement. Further, upon introducing displacements in the perturbed configurations, utilizing virtual displacements: the virtual axial displacement w_x, and the virtual transverse displacement w_y, and computing the Gâteaux derivative along the direction of these virtual displacements, the virtual von Karman deformation is derived as

$$\delta\varepsilon^{vk} = \frac{dw_x}{dx} + \frac{du_y}{dx}\frac{dw_y}{dx} - y\frac{d^2w_y}{dx^2} \tag{5}$$

In a classical manner, the weak form of the beam instability problem can be obtained by combining the well-known kinematic, constitutive, and equilibrium equations, resulting in the following expression

$$\int_l \left(\frac{dw_x}{dx} EA \frac{du_x}{dx} + \frac{d^2 w_y}{dx^2} EI \frac{d^2 u_y}{dx^2} \right) dx + \int_l \frac{dw_y}{dx} \frac{du_y}{dx} \underbrace{EA \left(\frac{du_x}{dx} \right)}_{N} dx = f^{ext} \tag{6}$$

A two-node beam finite element is employed next as the foundational framework for delineating the finite element approximation. Each node within this configuration has three degrees of freedom: two translational components, u_x and u_y, and one rotational component ϕ. The corresponding vectors of displacements and virtual displacements are

$$\begin{aligned} \mathbf{d}^T &= [u_{1x} \quad u_{1y} \quad \phi_1 \quad u_{2x} \quad u_{2y} \quad \phi_2]^{\mathrm{T}} \\ \mathbf{w}^T &= [w_{1x} \quad w_{1y} \quad w_1 \quad w_{2x} \quad w_{2y} \quad w_2]^{\mathrm{T}} \end{aligned} \tag{7}$$

The axial displacement field is described using linear shape functions N_i, while transverse displacements and rotations are characterised by Hermite shape functions H_i. The interpolations of the displacement fields are thus given as

$$\begin{aligned} u_x(x) &= N_1(x) u_{1x} + N_2(x) u_{2y} \\ u_y(x) &= H_1(x) u_{1y} + H_2(x) \phi_1 + H_3(x) u_{2y} + H_4(x) \phi_2 \end{aligned} \tag{8}$$

The same shape interpolations are also used for the virtual displacement field description. Further, one can easily obtain the corresponding derivatives of the displacement field and subsequently incorporate them into the Eq. (6), which results with the internal force vector

$$\begin{aligned} \mathbf{w}^T \mathbf{f}^{int} &= \mathbf{w}^T \underbrace{\int_l (\mathbf{N}^T EA \mathbf{N} + \mathbf{B}^T EI \mathbf{B}) dx}_{K_m} \mathbf{d} + \mathbf{w}^T \underbrace{\int_l \mathbf{H}^T \mathbf{H} N dx}_{K_g} \mathbf{d} = \mathbf{w}^T \mathbf{K}_m \mathbf{d} + \mathbf{w}^T \mathbf{K}_g \mathbf{d} \\ \mathbf{w}^T \mathbf{f}^{int} &= \mathbf{w}^T \left(\mathbf{K}_m + \mathbf{K}_g \right) \mathbf{d} \end{aligned} \tag{9}$$

where **N**, **B**, and **H** are defined as

$$\begin{aligned} \mathbf{N}^e &= \left[\frac{dN_1}{dx} \quad 0 \quad 0 \quad \frac{dN_2}{dx} \quad 0 \quad 0 \right] \\ \mathbf{H}^e &= \left[0 \quad \frac{dH_1}{dx} \quad \frac{dH_2}{dx} \quad 0 \quad \frac{dH_3}{dx} \quad \frac{dH_4}{dx} \right] \\ \mathbf{B}^e &= \left[0 \quad \frac{d^2 H_1}{dx^2} \quad \frac{d^2 H_2}{dx^2} \quad 0 \quad \frac{d^2 H_3}{dx^2} \quad \frac{d^2 H_4}{dx^2} \right] \end{aligned} \tag{10}$$

Following Eq. (9), the tangent stiffness matrix consists of the material stiffness matrix and the geometric stiffness matrix, written as

$$\begin{aligned} \mathbf{K}_t &= \mathbf{K}_m + \mathbf{K}_g \\ \mathbf{K}_m &= \int_l (\mathbf{N}^T EA \mathbf{N} + \mathbf{B}^T EI \mathbf{B}) dx \,;\ \mathbf{K}_g = \int_l \mathbf{H}^T \mathbf{H} N dx \end{aligned} \tag{11}$$

The material stiffness matrix for the case of a linear elastic material remains unchanged, while the geometric stiffness depends linearly on the applied load. Namely, the geometric stiffness matrix directly depends upon the axial force, that is, on the external loading. The external load can further be presented as the product of the load multiplier λ and the reference load value $\bar{\mathbf{f}}$, $\mathbf{f}^{ext} = \lambda\bar{\mathbf{f}}$. This fact can be further used to rewrite the geometric stiffness matrix as the product of the load multiplier λ and the reference value of geometric stiffness $\bar{\mathbf{K}}_g$ in the following manner

$$\mathbf{K}_t = \mathbf{K}_m + \lambda\bar{\mathbf{K}}_g \tag{12}$$

The reference value of geometric stiffness $\bar{\mathbf{K}}_g$ is computed for the reference value of the load $\bar{\mathbf{f}}$, resulting in the reference internal axial force $\bar{N}$

$$\bar{\mathbf{K}}_g = \int_l \mathbf{H}^T\mathbf{H}\bar{N}dx \tag{13}$$

The focus here lies in addressing instability phenomena characterised by the singularity of the stiffness matrix. The manifestation of instability suggests that small perturbations in applied loads may result in a disproportionately amplified response of the structure or of the structural element. Upon reaching a critical load, $\mathbf{f}_{cr} = \lambda_{cr}\bar{\mathbf{f}}$, the system attains a state of critical equilibrium. At this critical equilibrium state, the tangent stiffness matrix becomes singular, while its determinant assumes a zero value, written as

$$det\left(\mathbf{K}_m + \lambda_{cr}\bar{\mathbf{K}}_g\right) = 0 \tag{14}$$

To compute the critical load value, the solution of eigenvalue problem is used, defined as

$$\left(\mathbf{K}_m + \lambda_{cr}\bar{\mathbf{K}}_g\right)\boldsymbol{\psi}_{cr} = 0 \tag{15}$$

4. Numerical results

In this section, a set of numerical computations is performed in order to assess pile critical buckling force for various pile slenderness ratios and the undrained shear strength of surrounding soil, which is assumed to be soft clay. All numerical implementations and computations are carried out with the research version of the computer code FEAP, developed by R.L. Taylor (Zienkiewicz and Taylor 2005).

The numerical computations are performed for different diameters and lengths of pile resulting in a wide range of slenderness ratios. Namely, the outside diameter of the steel pipe pile is assumed constant in all computations and selected to be 80 mm, with a thickness equal to 8 mm. The pile length is varied at 2, 4, 8, 12, 16, and 20 m, resulting in a range od slenderness ratios from 25 to 250. Furthermore, additional computations were carried out for pile lengths less than 2 m to identify the slenderness ratio beyond which the critical buckling force remains unaffected.

The finite element mesh consists of geometrically nonlinear beam elements, each with a length of 0,1 m. Elastic springs are introduced at each finite element node to simulate the lateral support provided by the surrounding soil, i.e., the lateral pile-soil interaction. In all computations, the stiffness of the springs is uniformly set to $70c_u$, while the undrained shear strength is varied at 5, 10, 15, and 20 kPa. First, the assumption is made that the pile base rests on firm rock, and as a result, both the top and bottom ends of the pile in the numerical model are considered pin-

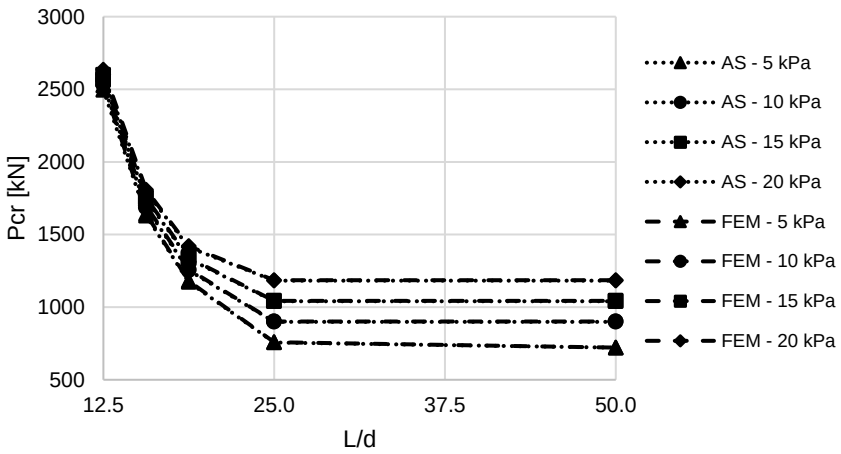

Fig. 3 Critical buckling force for slenderness ratios less than 50

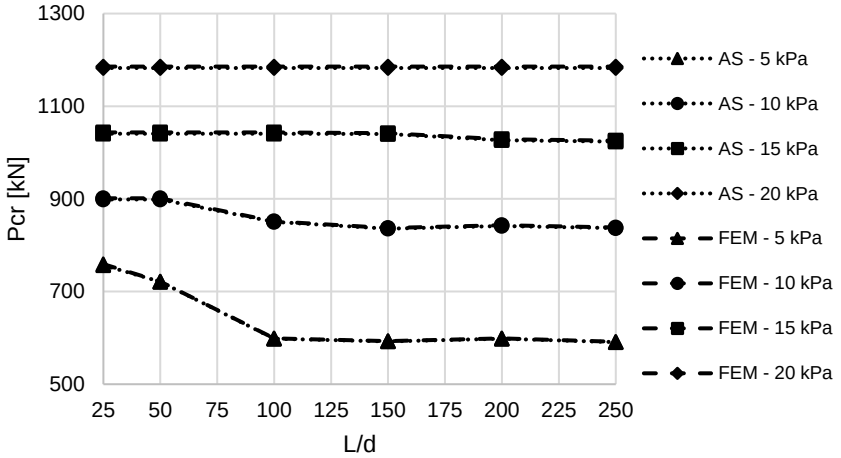

Fig. 4 Critical buckling force for slenderness ratios greater than 25

supported.

The computed critical buckling forces are shown in Fig. 3, for slenderness ratios less than 50, and in Fig. 4 for slenderness ratios greater than 25, for clear presentation of the results. The numerical results are compared against analytical solutions provided by Eq. (2). A high agreement between numerical and analytical results is obtained, which indicates a successful validation of the proposed numerical model under the specified conditions.

The results presented in Figs. 3 and 4 suggest that the reduction in the critical buckling force becomes significant for slenderness ratios greater than 25, for all values of undrained shear strength of surrounding soil. Above this value, for undrained shear strengths of 15 and 20 kPa, the critical buckling force does not change significantly with the change in slenderness ratio. However, for undrained shear strengths of 5 and 10 kPa, the limiting value of slenderness ratio, where further changes in critical buckling force are not significant, is approximately 100.

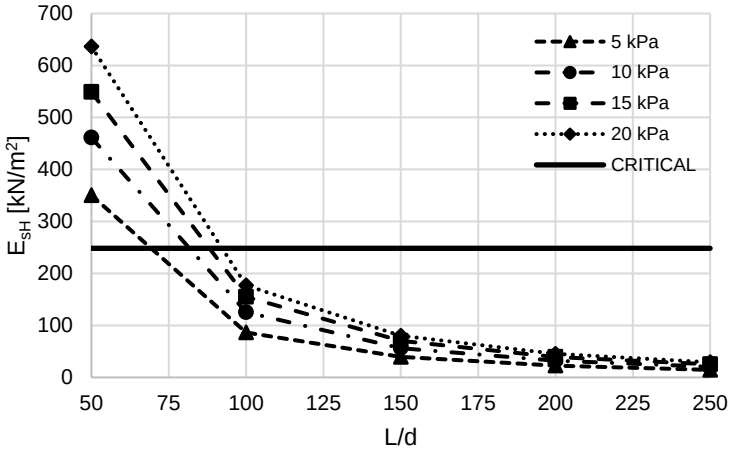

Fig. 5 Critical slenderness ratios when buckling should be evaluated further

To establish criteria when buckling should be evaluated further, the expression for the critical buckling force can be rewritten in the following manner (Bjerrum 1957)

$$P_{cr} = \frac{\pi^2 EI}{L^2} + \frac{E_{sH} L^2}{\pi^2} \tag{16}$$

Here, the first term corresponds to the Euler critical buckling force for unsupported pile, whereas the second term denotes the contribution of the lateral support provided by the surrounding soil, expressed now in terms of the modulus of lateral reaction of the soil E_{sH}.

Furthermore, the critical or limiting value of the modulus of lateral reaction of the soil, below which the possibility of the buckling should be evaluated further, can be determined from the following expression (Cadden and Gómez 2002)

$$E_{sH} \leq \frac{1}{\left[\left(4 \cdot \frac{I}{A^2}\right)\left(\frac{E}{f_y^2}\right)\right]} \tag{17}$$

where A is the cross-sectional area of the pile, and f_y is the yield stress of pile material.

The numerically obtained critical buckling forces are combined with Eq. (16) and (17) to obtain the critical slenderness ratios for which buckling should be examined more closely. The computed results are shown in Fig. 5, for yield stress of pile material equal to 275 MPa. The critical slenderness ratio tends to increase with an increase in the undrained shear strength of the surrounding soil. However, it is noteworthy that the critical slenderness ratio remains below 100, irrespective of the specific values chosen here for the undrained shear strength.

Next, the pile diameter is varied in order to obtain critical slenderness ratios for different pile cross-sectional properties. The computed results for the selected undrained shear strength of surrounding soil are shown in Fig. 6. As results confirm, the critical slenderness ratio for which the buckling should be analysed in more detail depends on both the pile and surrounding soil properties. Moreover, the identifid critical slenderness ratios fall within the typical range commonly encountered in micropiles used in engineering applications.

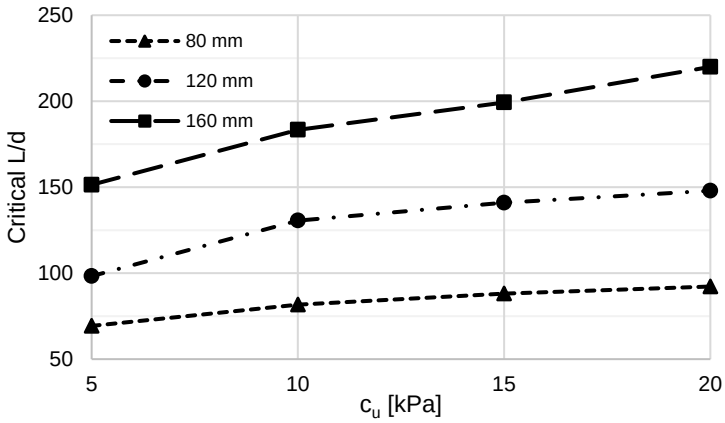

Fig. 6 Critical slenderness ratios for different pile diameters

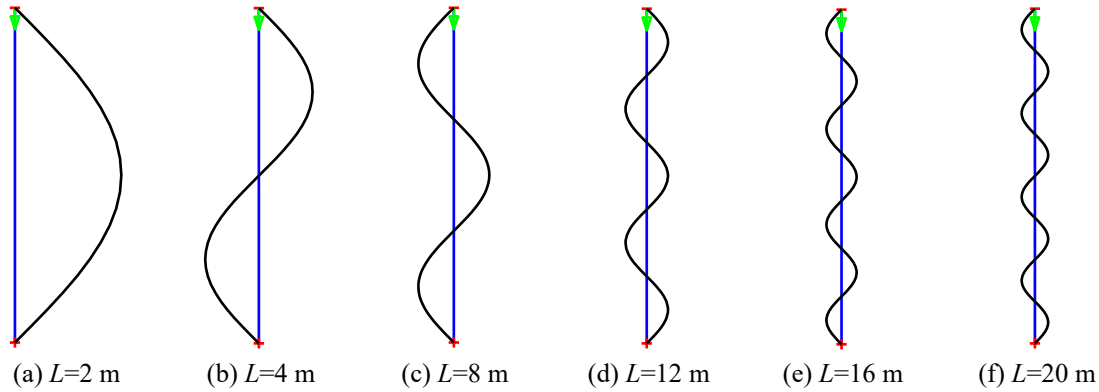

Fig. 7 Buckling modes, bottom end of the pile pin-supported, d=80 mm, c_u=10 kPa

The buckling modes for different pile lengths match those obtained analytically and are shown in Fig. 7 (a)-(f).

Next, the entire length of the pile (d=80 mm) is assumed to be in weak soil, corresponding to the conditions typically associated with floating piles. Initially, the case of a fully-floating pile is considered, thereby resulting in a free bottom end of the pile. For numerical purposes, the vertical spring with a very small stiffness is introduced at the bottom end of the pile. Subsequently, the contribution of the pile base is taken into account by introducing a vertical spring at the bottom end of the pile, with its stiffness determined using the following expression (Crispin and Mylonakis 2021)

$$k_v = \frac{E_s d}{(1 - \nu_s^2)} \tag{18}$$

where E_s is the soil modulus of elasticity at the pile base, d is the pile diameter, and ν_s is the Poisson ratio of soil, which for soft clays can be taken as 0,2.

The soil modulus of elasticity E_s is derived from the undrained modulus of elasticity of soil, which, in turn, is determined by correlating it with undrained shear strength. The undrained

Table 1 The vertical spring stiffness values

Undrained shear strength	Undrained modulus of elasticity of soil	Modulus of elasticity of soil	Vertical spring stiffness
c_u [kPa]	E_u [kPa]	E_s [kPa]	k_v [kN/m]
5	4000	3200	266,67
10	8000	6400	533,33
15	12000	9600	800,00
20	16000	12800	1066,67

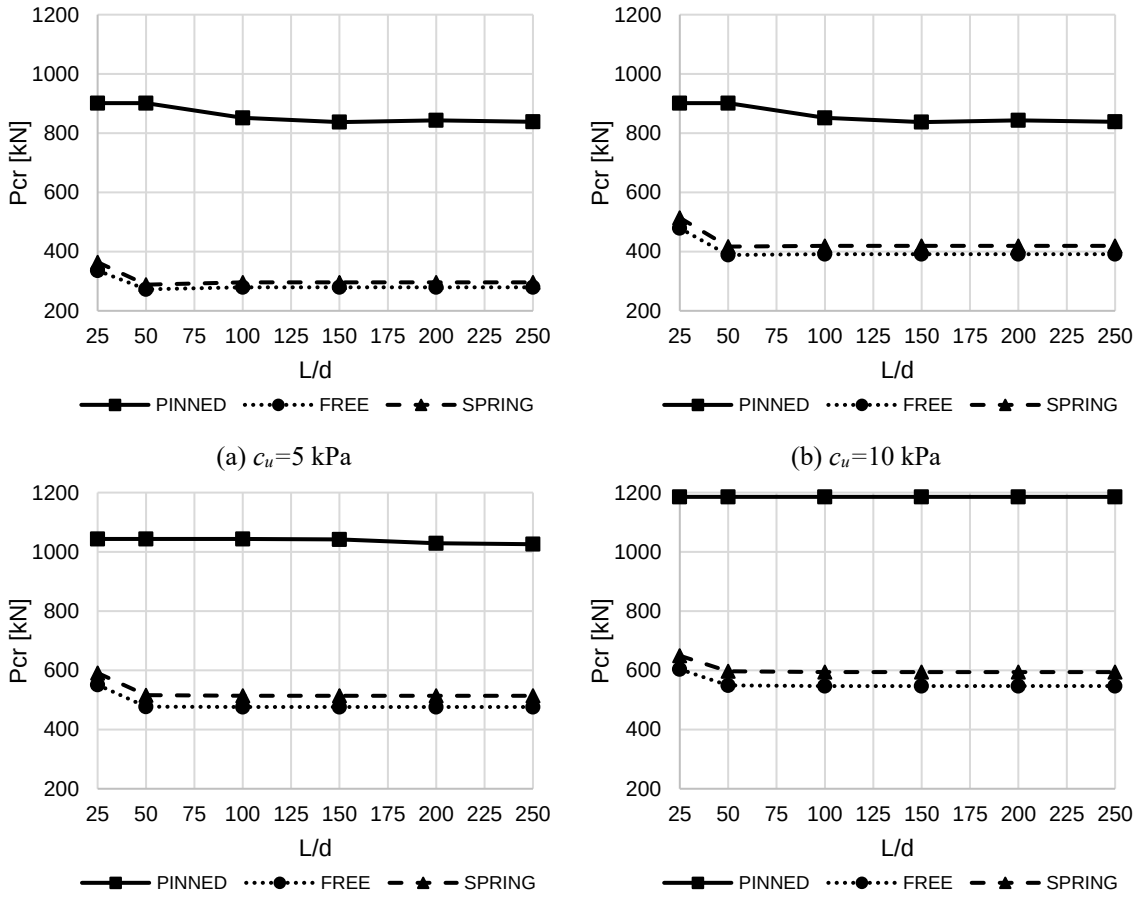

(a) c_u=5 kPa (b) c_u=10 kPa

(c) c_u=15 kPa (d) c_u=20 kPa

Fig. 8 Critical buckling force for different pile bottom end boundary conditions

modulus of elasticity is considered equal to E_u=800c_u. The soil modulus of elasticity E_s is then equal to

$$E_s = \frac{2(1+\nu_s)}{3} E_u \tag{19}$$

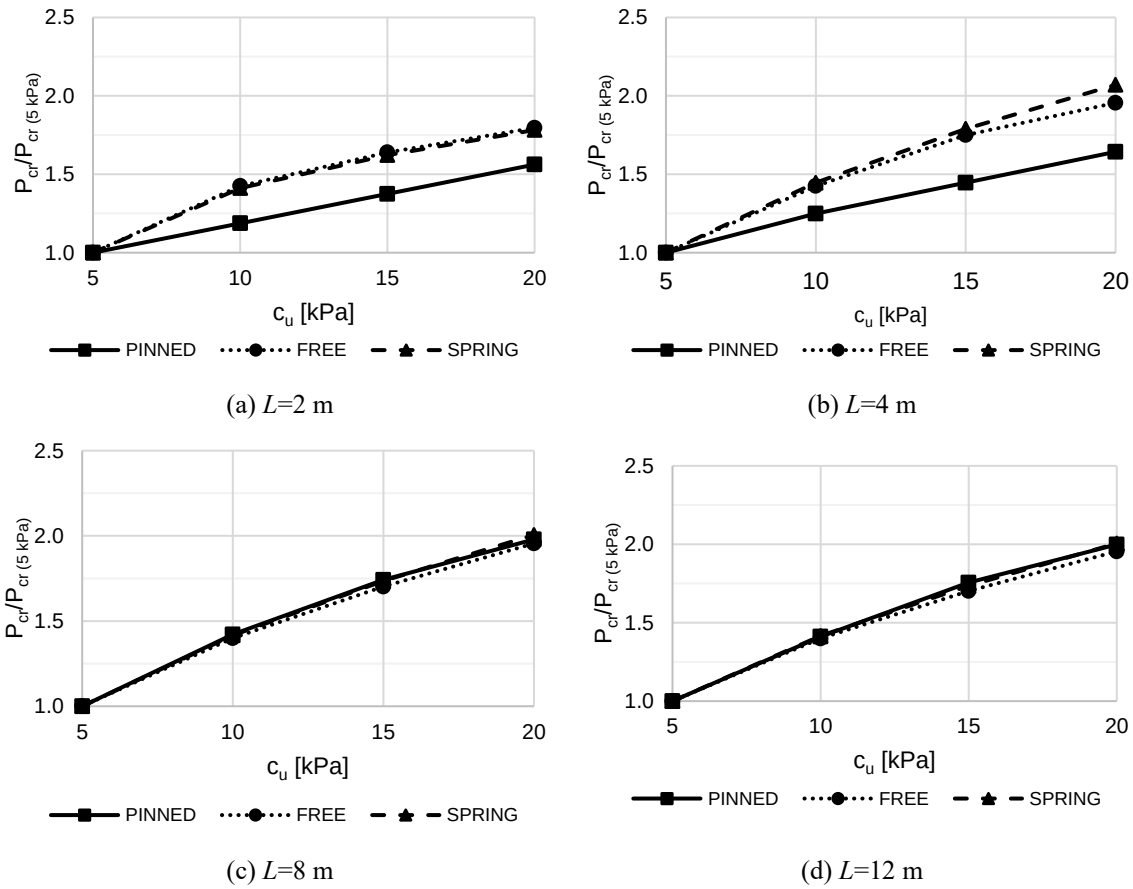

Fig. 9 Increase trends in critical buckling force for selected undrained shear strength values

The computed vertical spring stiffness values are given in Table 1.

The comparison of computed results for three types of pile bottom end boundary conditions and for different values of undrained shear strength of soil are shown in Fig. 8 (a)-(d). The results indicate that the critical buckling force for floating piles is approximately half of that computed for piles pinned at the bottom end. The addition of a vertical spring with stiffness values calculated from Eq. (15), simulating the contribution of the pile base, does not affect the critical buckling force significantly when compared to the case of fully-floating piles. Namely, due to the generally small diameter and, consequently, small cross-sectional area, any bottom end contribution in micropiles embedded in weak soil can be neglected.

The influence of undrained shear strength of the surrounding soil on the critical buckling force for all three types of pile bottom end boundary conditions and for pile lengths of 2, 4, 8, and 12 m is shown in Fig. 9 (a)-(d). A consistent trend in the influence of undrained shear strength on the critical buckling force is observed for pile lengths of 8 and 12 m for all varied pile bottom end boundary conditions. Similar trends are also obtained for pile lengths of 16 and 20 m. However, for 2 and 4 m pile lengths, the trend obtained for free and spring-supported pile bottom end differs from that obtained for pin-supported bottom end. Specifically, for these pile lengths, an increase in

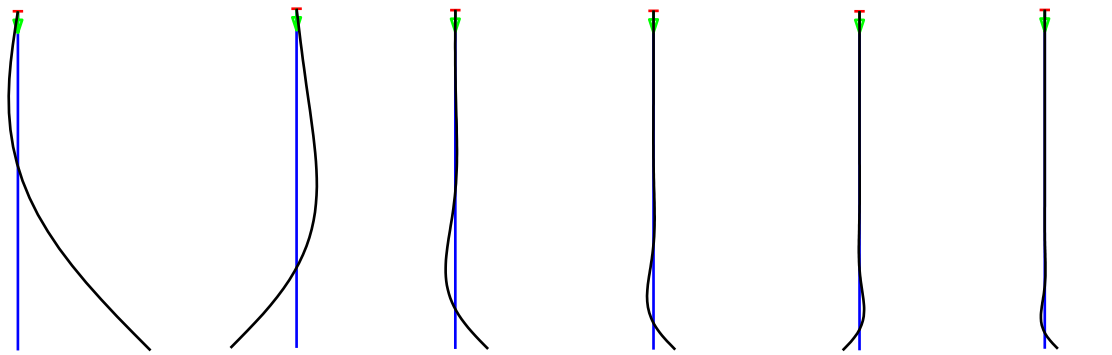

(a) L=2 m (b) L=4 m (c) L=8 m (d) L=12 m (e) L=16 m (f) L=20 m

Fig. 10 Buckling modes, bottom end of the pile spring-supported, d=80 mm, c_u=10 kPa

soil undrained shear strength has a comparatively lesser impact on the critical buckling force when the bottom end of the pile is pinned.

The buckling modes for spring-supported pile bottom end for different pile lengths are shown in Fig. 10 (a)-(f). A similar is obtained for the free bottom end of the pile.

5. Conclusions

In this paper, a novel numerical model that advances the understanding of pile buckling by incorporating beam elements and explicitly considering geometric nonlinearities through the von Karman deformation measure is presented. Its ability to consider geometric nonlinearities provides a more realistic representation of pile buckling behavior, offering valuable insights for the design and assessment of piles.

The model capabilities are tested across a range of pile slenderness ratios and soil conditions. The validation of the numerical model is achieved by comparing the computed critical buckling forces against existing analytical solutions, revealing a high level of agreement. The critical slenderness ratios determined for selected pile properties and undrained shear strength values of the surrounding soil fall within the range of slenderness ratios typically seen in micropiles commonly used in engineering applications. The influence of pile bottom end boundary conditions is also examined, unveiling that the critical buckling force for floating piles is reduced by almost half compared to the case when the pile base is on firm rock. Floating piles are also commonly observed in engineering practice. These observations combined indicate that the potential for pile buckling in weaker soils, such as soft clays, should be recognized and not underestimated. They emphasize the importance of considering buckling phenomena in the design and analysis of micropiles, particularly in conditions where weak soils are prevalent.

References

Bergfelt, A. (1957), "The axial and lateral load bearing capacity, and failure by buckling of piles in soft clay", *Proc. 4th Int. Conf. on Soil Mechanics and Foundation Engineering*, London, **2**, 8-13.

Bhattacharya, S., Carrington, T.M. and Aldridge, T.R. (2005), "Buckling considerations in pile design",

Proceedings of the International Symposium on Frontiers in Offshore Geotechnics, 815-821.

Bjerrum, L. (1957), "Norwegian experiences with steel piles to rock", *Geotechnique*, **7**(2), 73-96. https://doi.org/10.1680/geot.1957.7.2.73.

Bruce, D.A., Cadden, A.W. and Sabatini, P.J. (2005), "Practical advice for foundation design-micropiles for structural support", *Contemporary Issues in Foundation Engineering*, 1-25.

Cadden, A.W. and Gómez, J.E. (2002), "Buckling of micropiles-a review of historic research and recent experiences", ADSC-IAF Micropile Committee.

Chen, Y.H., Chen, L., Xu, K., Liu, L. and Ng, C.W.W. (2013), "Study on critical buckling load calculation method of piles considering passive and active earth pressure", *Struct. Eng. Mech.*, **48**(3), 367-382. https://doi.org/10.12989/sem.2013.48.3.367.

Crispin, J.J. and Mylonakis, G.E. (2021), "Simplified models for axial static and dynamic analysis of pile foundations", *Analysis of Pile Foundations Subject to Static and Dynamic Loading*, CRC Press.

Davisson, M.T. (1963), "Estimating buckling loads for piles", *Proceedings of the 2nd Pan-American Conference on Soil Mechanics and Foundation Engineering*, Brazil, **2**, 351-369.

Engesser, F. (1889), *Uber Knickfestigkeit Gerader Stabe*, Verlag Von Wilhelm Ernst & Sohn, Berlin, Germany.

Gabr, M.A., Wang, J.J. and Zhao, M. (1997), "Buckling of piles with general power distribution of lateral subgrade reaction", *J. Geotech. Geoenviron. Eng.*, **123**(2), 123-130. https://doi.org/10.1061/(ASCE)1090-0241(1997)123:2(123).

Gatto, M.P.A. and Montrasio, L. (2021), "Analysis of the behaviour of very slender piles: focus on the ultimate load", *Int. J. Civil Eng.*, **19**, 145-153. https://doi.org/10.1007/s40999-020-00547-y.

Hajdo, E., Hadzalic, E. and Ibrahimbegovic, A. (2022), "Linear Buckling Analysis of Structures on the Elastic Support", *International Symposium on Innovative and Interdisciplinary Applications of Advanced Technologies*, 92-102.

Hajdo, E., Ibrahimbegovic, A. and Dolarevic, S. (2020), "Buckling analysis of complex structures with refined model built of frame and shell finite elements", *Couple. Syst. Mech.*, **9**(1), 29-46. https://doi.org/10.12989/csm.2020.9.1.029.

Hajdo, E., Mejia-Nava, R.A., Imamovic, I. and Ibrahimbegovic, A. (2021), "Linearized instability analysis of frame structures under nonconservative loads: Static and dynamic approach", *Couple. Syst. Mech.*, **10**(1), 79. https://doi.org/10.12989/csm.2021.10.1.079.

Heelis, M.E., Pavlović, M.N. and West, R.P. (2004), "The analytical prediction of the buckling loads of fully and partially embedded piles", *Geotechnique*, **54**(6), 363-373. https://doi.org/10.1680/geot.2004.54.6.363.

Hegazy, A.A.E. (2014), "Analysis of buckling load micropiles embedded in a weak soil under vertical axial loads", *Int. J. Civil Eng.*, **3**, 155-166.

Ibrahimbegovic, A. (2009), *Nonlinear Solid Mechanics: Theoretical Formulations and Finite Element Solution Methods*, Springer, Berlin, Germany.

Ibrahimbegović, A. and Frey, F. (1993), "Finite element analysis of linear and non-linear planar deformations of elastic initially curved beams", *Int. J. Numer. Meth. Eng.*, **36**(19), 3239-3258. https://doi.org/10.1002/nme.1620361903.

Ibrahimbegovic, A., Hajdo, E. and Dolarevic, S. (2013), "Linear instability or buckling problems for mechanical and coupled thermomechanical extreme conditions", *Couple. Syst. Mech.*, **2**(4), 349-374.

Imamovic, I., Ibrahimbegovic, A. and Hajdo, E. (2019), "Geometrically exact initially curved Kirchhoff's planar elasto-plastic beam", *Couple. Syst. Mech.*, **8**(6), 537-553. https://doi.org/10.12989/csm.2019.8.6.537.

Jelenić, G. and Crisfield, M. (1999), "Geometrically exact 3D beam theory: Implementation of a strain-invariant finite element for statics and dynamics", *Comput. Meth. Appl. Mech. Eng.*, **171**(1-2), 141-171. https://doi.org/10.1016/S0045-7825(98)00249-7.

Knappett, J.A. and Madabhushi, S.P.G. (2009), "Influence of axial load on lateral pile response in liquefiable soils. Part II: numerical modelling", *Géotechnique*, **59**(7), 583-592. https://doi.org/10.1680/geot.8.009.3749.

Masjedi, P.K., Maheri, A. and Weaver, P.M. (2019), "Large deflection of functionally graded porous beams

based on a geometrically exact theory with a fully intrinsic formulation", *Appl. Math. Model.*, **76**, 938-957. https://doi.org/10.1016/j.apm.2019.07.018.

Meier, C., Popp, A. and Wall, W.A. (2019), "Geometrically exact finite element formulations for slender beams: Kirchhoff-Love theory versus Simo-Reissner theory", *Arch. Comput. Meth. Eng.*, **26**(1), 163-243. https://doi.org/10.1007/s11831-017-9232-5.

Mejia-Nava, R.A., Imamovic, I., Hajdo, E. and Ibrahimbegovic, A. (2022), "Nonlinear instability problem for geometrically exact beam under conservative and non-conservative loads", *Eng. Struct.*, **265**, 114446. https://doi.org/10.1016/j.engstruct.2022.114446.

Nadeem, M., Chakraborty, T. and Matsagar, V. (2015), "Nonlinear buckling analysis of slender piles with geometric imperfections", *J. Geotech. Geoenviron. Eng.*, **141**(1), 06014014. https://doi.org/10.1061/(ASCE)GT.1943-5606.0001189.

Ofner, R. and Wimmer, H. (2007), "Buckling resistance of micropiles in varying soil layers", *Bautechnik*, **84**(12), 881-890.

Poulos, H.G. and Davis, E.H. (1980), *Pile Foundation Analysis and Design*, Vol. 397, Wiley, New York.

Prakash, S. (1987), "Buckling loads of fully embedded vertical piles", *Comput. Geotech.*, **4**(2), 61-83. https://doi.org/10.1016/0266-352X(87)90011-5.

Reese, L.C., Wang, S.T., Isenhower, W.M., Arrellaga, J.A., Hendrix, J. (2000), LPILE Plus Version 4.0 Technical Manual, Ensoft Inc., Austin, USA.

Sabatini, P.J., Armour, T., Groneck, P., Keeley, J.W. and Tanyu, B. (2005), "Micropile design and construction (reference manual for NHI Course 132078) (No. FHWA-NHI-05-039)", Department of Transportation. Federal Highway Administration, United States.

Timoshenko, S.P. and Gere, J.M. (1961), *Theory of Elastic Stability*, McGraw-Hill, New York.

Tojaga, V., Kulachenko, A., Östlund, S. and Gasser, T.C. (2021), "Modeling multi-fracturing fibers in fiber networks using elastoplastic Timoshenko beam finite elements with embedded strong discontinuities-Formulation and staggered algorithm", *Comput. Meth. Appl. Mech. Eng.*, **384**, 113964. https://doi.org/10.1016/j.cma.2021.113964.

Vogt, N., Vogt, S. and Kellner, C. (2009), "Buckling of slender piles in soft soils", *Bautechnik*, **86**(S1), 98-112. https://doi.org/10.1002/bate.200910046.

Zhang, X., Tang, L., Ling, X. and Chan, A. (2020), "Critical buckling load of pile in liquefied soil", *Soil Dyn. Earthq. Eng.*, **135**, 106197. https://doi.org/10.1016/j.soildyn.2020.106197.

Zhao, M.H., He, W. and Li, Q.S. (2010), "Post-buckling analysis of piles by perturbation method", *Struct. Eng. Mech.*, **35**(2), 191-203. https://doi.org/10.12989/sem.2010.35.2.191.

Zienkiewicz, O.C. and Taylor, R.L. (2005), *The Finite Element Method*, Vols. I, II, III, Elsevier.

CC